Design Optimization and Implementation for RF Energy Harvesting Circuits

Prusayon Nintanavongsa, *Student Member, IEEE*, Ufuk Muncuk, David Richard Lewis, and Kaushik Roy Chowdhury, *Member, IEEE*

***Abstract*—A new design for an energy harvesting device is proposed in this paper, which enables scavenging energy from radio-frequency (RF) electromagnetic waves. Compared to common alternative energy sources like solar and wind, RF harvesting has the least energy density. The existing state-of-the-art solutions are effective only over narrow frequency ranges, are limited in efficiency response, and require higher levels of input power. This paper has a twofold contribution. First, we propose a dual-stage energy harvesting circuit composed of a seven-stage and ten-stage design, the former being more receptive in the low input power regions, while the latter is more suitable for higher power range. Each stage here is a modified voltage multiplier, arranged in series and our design provides guidelines on component choice and precise selection of the crossover operational point for these two stages between the high (20 dBm) and low power (−20 dBm) extremities. Second, we fabricate our design on a printed circuit board to demonstrate how such a circuit can run a commercial Mica2 sensor mote, with accompanying simulations on both ideal and non-ideal conditions for identifying the upper bound on achievable efficiency. With a simple yet optimal dual-stage design, experiments and characterization plots reveal approximately 100% improvement over other existing designs in the power range of −20 to 7 dBm.**

***Index Terms*—Optimization, power efficiency, radio-frequency (RF) energy harvesting circuit, Schottky diode, sensor, voltage multiplier, 915 MHz.**

I. Introduction

With the growing popularity and applications of large-scale, sensor-based wireless networks (e.g., structural health monitoring, human health monitoring, to name a couple), the need to adopt inexpensive, green communications strategies is of paramount importance. One approach is to deploy a network comprising self-powered nodes, i.e., nodes that can harvest ambient energy from a variety of natural and man-made sources for sustained network operation [5]. This can instrument potentially leading to significant reduction in the costs associated with replacing batteries periodically. Moreover, in some deployments, owing to the sensor location, battery replacement may be both practically and economically infeasible, or may involve significant risks to human life. Thus, there is a strong motivation to enable an off-the-shelf wireless sensor network (WSN) with energy harvesting capability that would allow a sensor to replenish part or all of its operational costs, thereby taking the first steps towards realizing the vision of a perennially operating network.

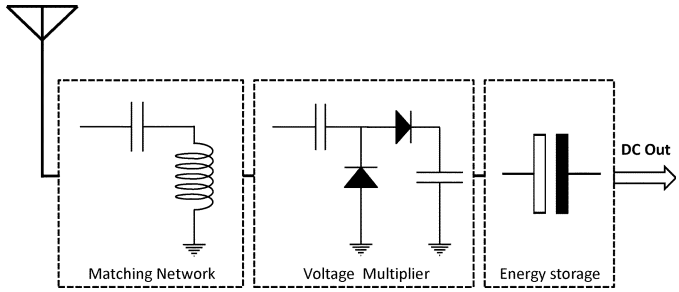

Fig. 1. Ambient RF energy harvesting.

The concept of wireless energy harvesting and transfer is not new, rather it was demonstrated over 100 years ago by Tesla [1]. In recent times, RFID technology is a clear example of wireless power transmission where such a tag operates using the incident radio-frequency (RF) power emitted by the transmitter [2]. However, there are limitations in directly porting these approaches to WSN scenarios: the former cannot be scaled down for the small form factor sensors, while RFID is unable to generate enough energy to run the local processing tasks on the node, such as powering the Atmel ATmega128L microcontroller on the MICA2 mote (Crossbow Technology, Milpitas, CA) . However, given the recent advances in energy efficiency for the circuit components of a sensor (say, diodes that require less forward voltage threshold), and the low-power operation modes supported by the device itself (say, sleep mode consuming only millivolt), there is a visible need for revisiting energy harvesting circuit design that can successfully operate a sensor node.

Fig. 1 shows the components of our proposed energy harvesting circuit. The incident RF power is converted into dc power by the voltage multiplier. The matching network, composed of inductive and capacitive elements, ensures the maximum power delivery from antenna to voltage multiplier. The energy storage ensures smooth power delivery to the load, and as a reserve for durations when external energy is unavailable. Such a design needs to be carefully crafted: increasing the number of multiplier stages gives higher voltage at the load, and yet reduces the current through the final load branch. This may result in unacceptable charging delays for the energy storage capacitor. Conversely, fewer stages of the multiplier will ensure

Manuscript received October 15, 2011; revised January 12, 2012; accepted January 30, 2012. Date of publication February 28, 2012; date of current version April 11, 2012. This material is based upon work supported by the U.S. National Science Foundation under Grant CNS-1143662.

The authors are with the Department of Electrical and Computer Engineering, Northeastern University, Boston, MA 02115 USA (e-mail: prusayon@ece.neu.edu; umuncuk@ece.neu.edu; dlewis@ece.neu.edu; krc@ece.neu.edu).

Color versions of one or more of the figures in this paper are available online at http://ieeexplore.ieee.org.

Digital Object Identifier 10.1109/JETCAS.2012.2187106

quick charging of the capacitor, but the voltage generated across it may be insufficient to drive the sensor mote (at least 1.8V that becomes the $+$Vcc for Mica2 sensors). Along similar lines, a slight change in the matching circuit parameters alters significantly the frequency range in which the efficiency of the energy conversion is maximum, often by several megahertz. Hence, RF harvesting circuits involve a complex interplay of design choices, which must be considered together. We address this problem by considering a multistage design of the voltage multiplier, whose operating points are decided by solving an optimization framework. We summarize the main contributions of our work as follows.

- We propose a circuit design tuned to the unlicensed ISM band at 915 MHz[1] composed of commonly available off-the-shelf components, such as zero bias Schottky diodes HSMS-2822 and HSMS-2852 (Avago Technologies, San Jose, CA) , with printed circuit boards (PCBs) that can be fabricated at marginal costs. This will ultimately result in mass deployment of harvesting boards along with the sensor nodes.
- We propose a dual-stage design, one that is most efficient at extremely low input RF power [say, low-power design (LPD)], and the other at comparatively higher range [say, high-power design (HPD)]. We develop an optimization framework to decide the switchover point between these two sister-circuits so that the fabricated circuit as a whole delivers the highest achievable efficiency in the operational incident power range of -20 to 20 dBm.
- We demonstrate the interfacing of our circuit with a commonly available Mica2 sensor mote, and then characterize through experiments, the impact on the duty cycle of such an integrated device that is powered by harvesting alone.
- We undertake a rigorous performance evaluation and compare the design solutions from simulation, under ideal and nonideal conditions, with the real PCB fabrication, and also with the state of the art commercially available products in terms of efficiency and generated voltage. The nonideal simulation provides a bound on achievable efficiency with respect to a particular design.
- We propose the use of multiple input antennas to increase the amount of energy harvested. The simulation result shows that it is feasible although there exists a bound on numbers of antennas implemented.

The rest of this paper is organized as follows. In Section II, we describe the related work, followed by discussion on the component selection for the energy harvesting circuit in Section III. The optimization framework is described in Section IV. The simulation results are presented in Section V. In Section VI, we describe the challenges and solutions in fabricating the energy harvesting circuit with parameters obtained from the simulation. We also undertake the performance evaluation of the fabricated circuit in Section VI, as well. Finally, Section VII concludes our work.

[1]The 915 MHz ISM band is chosen as it allows direct comparison with the commercial solution from Powercast [16], also operating in the same band. Our design can be tuned to other frequency ranges as well.

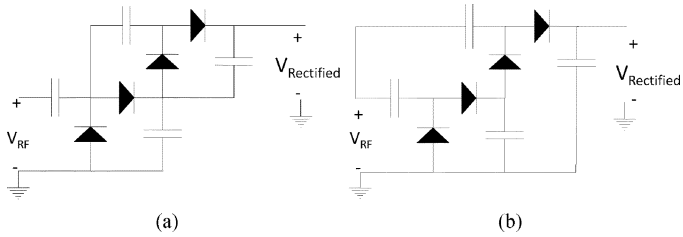

Fig. 2. (a) Villard multiplier and (b) Dickson multiplier.

II. Related Work

Energy harvesting has been in the focus of the research community in recent years. There are numerous sources of power that energy harvesting can benefit from, and solar energy harvesting is one of the key examples since it has the highest energy density among other candidates. However, it has a drawback of being able to operate only when sunlight is present. In [5], a solar energy harvesting module is used to power a sensor mote. Vibrational energy harvesting is presented in [3] while harvesting energy from thermoelectric device attached to human is discussed in [4]. Small amount of work has been done on RF energy harvesting due to its low energy density. Wireless battery charging system using radio frequency energy harvesting is discussed in [7]. RF energy harvesting with ambient source is presented in [8] where energy harvester can obtain 109 μW of power from daily routine in Tokyo. In [6], the energy of 60 μW is harvested from TV towers, 4.1 km away, and is able to operate small electronic device. Ambient RF energy harvesting with two systems has been studied in [15]. The first is broadband system without matching while the second is narrow band with matching. The preliminary results indicate that the harvested energy is not sufficient to directly power devices but could be stored for later use. In [19], the authors investigate the feasibility and potential benefits of using passive RFID as a wake-up radio. The results show that using a passive RFID wake-up radio offers significant energy efficiency benefits at the expense of delay and the additional low-cost RFID hardware. Recently prototypes for such RF harvesters have been developed in the academia [9], [10], as well as commercial products have been introduced by the industry [16]. However, we have evaluated the Powercast lifetime power evaluation and development kit and it does not perform well under an RF environment, with incident power 0 dBm and lower. Consequently, there is a need to develop an energy harvesting circuit that performs well under these low power conditions.

Our proposed RF energy harvesting circuit is based on the voltage multiplier circuit, which was invented by Heinrich Greinacher in 1919. Later in 1951, Cockcroft and Walton used this concept in their research to accelerate particles to study the atomic nucleus and were awarded a Nobel Prize in Physics. A basic schematic of a Villard voltage doubler, sometimes also called Cockcroft–Walton voltage multiplier, and Dickson voltage multiplier are shown in Fig. 2(a) and (b), respectively. According to [12], Both Villard and Dickson topology reveal no significant difference in performance.

III. RF Energy Harvesting Circuit Components

The main challenge faced in harvesting RF energy is the free-space path loss of the transmitted signal with distance. The Friis transmission equation relates the received (P_r) and transmitted (P_t) powers with the distance R as

$$P_r = P_t G_t G_r \left(\frac{\lambda}{4\pi R}\right)^2 \quad (1)$$

where G_t and G_r are antenna gains, and λ is the wavelength of the transmitted signal. The received signal strength, diminishes with the square of the distance, requires special sensitivity considerations in the circuit design. Moreover, FCC regulations limit the maximum transmission power in specific frequency bands. For example, in the 900-MHz band, this maximum threshold is 4 W [11]. Even at this highest setting, the received power at a moderate distance of 20 m is attenuated down to only 10 μW. We describe a new circuit design in this section that is capable of scavenging energy with high efficiency, beginning with the selection of the circuit components. We choose the Dickson topology [Fig. 2(b)] as the parallel configuration of capacitors in each stage reduces the circuit impedance, and hence makes the matching task simpler. In the following, we describe the parameters that influence selection of the circuit components, and the design strategies for efficiency in performance.

A. Choice of Diodes

One of the crucial requirements for the energy harvesting circuit is to be able to operate with weak input RF power. For a typical 50-Ω antenna, the -20 dBm received RF signal power means an amplitude of 32 mW. As the peak voltage of the ac signal obtained at the antenna is generally much smaller than the diode threshold [12], diodes with lowest possible turn on voltage are preferable. Moreover, since the energy harvesting circuit is operating in high frequencies, diodes with a very fast switching time need to be used. Schottky diodes use a metal–semiconductor junction instead of a semiconductor–semiconductor junction. This allows the junction to operate much faster, and gives a forward voltage drop of as low as 0.15 V. In this paper, we employ two different diodes from Avago Technologies, HSMS-2822 and HSMS-2852. The former has the turn on voltage of 340 mV while the latter is at 150 mV, measured at 1 and 0.1 mV, respectively. Consequently, HSMS-2852 is suitable for LPD used in the weak RF environment, while HSMS-2822 is preferred for HPD in the strong RF environment. Saturation current is another critical parameter that impacts the efficiency of diodes. It is desirable to have diodes with high saturation current, low junction capacitance, and low equivalent series resistance (ESR). Moreover, diodes with higher saturation current also yield higher forward current, which is beneficial for load driving. However, higher saturation current is usually found in larger diodes, which have higher junction and substrate capacitance. The latter two parameters can introduce increased power loss, where the benefit of higher saturation current is lost.

B. Number of Stages

The number of rectifier stages has a major influence on the output voltage of the energy harvesting circuit. Each stage here is a modified voltage multiplier, arranged in series. The output voltage is directly proportional to the number of stages used in the energy harvesting circuit. However, practical constraints force a limit on the number of permissible stages, and in turn, the output voltage. Here, the voltage gain decreases as number of stages increases due to parasitic effect of the constituent capacitors of each stage, and finally it becomes negligible. Figs. 3 and 4 show the impact of number of stages on efficiency and output voltage of energy harvesting circuit, respectively. We have used Agilent ADS with parameters sweep of -20 to 20 dBm for the input RF power and varies numbers of circuit stages from 1 to 9 stages. The circuit stage in simulation is a modified voltage multiplier of HSMS-2852, arranged in series. We observe that the circuit yields higher efficiency as the number of stages increases. However, as more stages are introduced, the peak of the efficiency curve also shifts towards the higher power region. The voltage plot shows that higher voltage can be achieved by increasing number of circuit stages, but a corresponding increase in power loss is also introduced into the low power region.

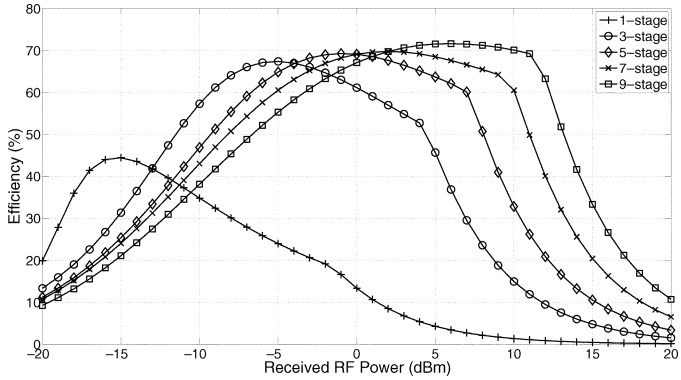

Fig. 3. Effect of number of stages on the efficiency of energy harvesting Circuit.

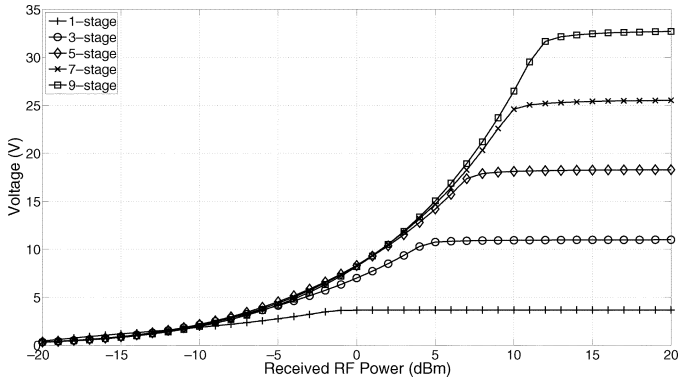

Fig. 4. Effect of number of stages on the output voltage of energy harvesting Circuit.

C. Effect of Load Impedance

It is important that the load impedance be carefully selected for a specific energy harvesting circuit, whose impact on the circuit performance can be seen in Fig. 5. We simulate the effect of load impedance on the efficiency of the energy harvesting circuit using Agilent ADS with parameters sweep of -20 to 20 dBm and 1–181 KΩ for input RF power and load value, respectively.

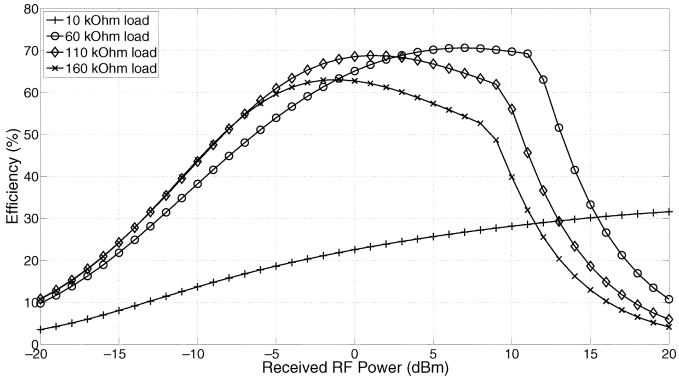

Fig. 5. Effect of load impedance on the efficiency of energy harvesting circuit.

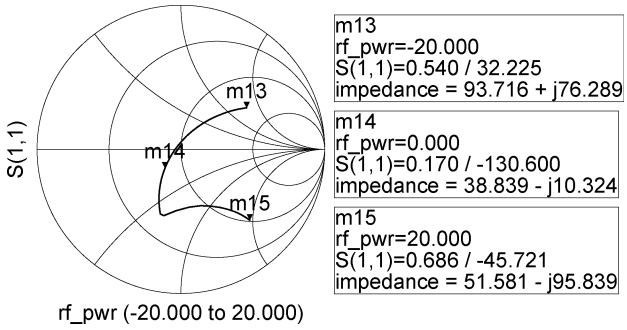

Fig. 6. Effect of RF input power on the impedance of the energy harvesting circuit.

We observe that the circuit yields the optimal efficiency at a particular load value, that is, the circuit's efficiency decreases dramatically if the load value is too low or too high. The energy harvesting in simulation is five-stage circuit, each stage is a modified voltage multiplier of HSMS-2852, arranged in series. For the particular case of WSNs, the sensor mote draws a different amount of current when it in the active (all radios operational), low-power (radios shut down for short interval but internal microcontroller active), and deep-sleep (requires external interrupt signal to become active again) states. To correctly identify the impedance in the deep sleep state, where we presume the node harvests energy, we measure the voltage and current of Mica2 sensor mote in deep sleep state to consume 30 μA at 3.0 V, which translates to a 100-KΩ resistive load. A 100-KΩ resistive load is further used in our optimization.

D. Effect of RF Input Power

Since the energy harvesting circuit consists of diodes, which are nonlinear devices, the circuit itself exhibits nonlinearity. This implies that the impedance of the energy harvesting circuit varies with the amount of power received from the antenna. Since the maximum power transfer occurs when the circuit is matched with the antenna, the impedance matching is usually performed at the a particular input power. Fig. 6 depicts the effect of RF input power, ranging from -20 to 20 dBm, on the impedance of the energy harvesting circuit. The nonlinearity in operation is shown by a sharp bend at 5 dBm. This further motivates our approach of a clear separation of two optimized sister-circuits of the LDP and HDP, where each has its own (reasonably) constant impedance.

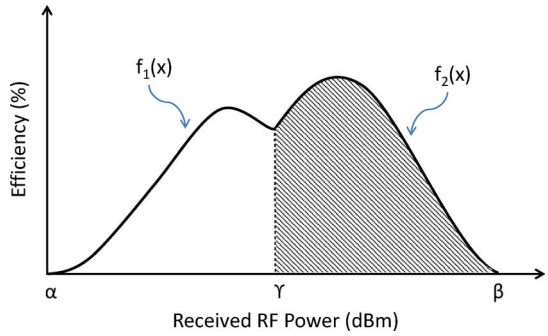

Fig. 7. Efficiency curves of two energy harvesting sister-circuits, for LPD and HPD.

IV. Optimization Framework

The aim of this optimization framework is to maximize the efficiency of the energy harvesting module throughout the range of -20 to 20 dBm, subject to several device and performance constraints. The conversion efficiency is defined in [14] as

$$\eta_c = \frac{\text{DC Output Power}}{\text{Incident RF Power} - \text{Reflected RF Power}}, \quad (2)$$

whereas, the overall efficiency is given by

$$\eta_o = \frac{\text{DC Output Power}}{\text{Incident RF Power}}. \quad (3)$$

Conversion efficiency is defined as a ratio of dc output power of energy harvesting circuit to net RF input power incident at the input end of the circuit. Consider a plot that measures the efficiency of the circuit against the input power, also called as the *efficiency curve*. The intersection of the two efficiency curves of the LPD (using the HSMS-2852 diode) and HPD (using the HSMS-2822 diode) circuits, called as the *crossover point*, splits the overall target range of -20 to 20 dBm into two.

Conversion efficiency does not take impedance mismatch into the account, and hence reflected power is subtracted from received power from the antenna. Consequently, conversion efficiency is a good parameter to measure the efficiency of only the adaptations we propose in the voltage multiplier circuit. On the contrary, overall efficiency is defined as a ratio of dc output power of energy harvesting circuit to incidental RF power at the antenna. It also includes the effect of reflected RF in the calculation. Therefore, overall efficiency provides a complete representation of the energy harvesting circuit performance, since matching network is also considered in the efficiency calculation. We use the overall efficiency η_o as the main performance metric in this paper according to this reason, which is the sum of two curves on either side of the crossover point.

Fig. 7 shows the two efficiency curves of energy harvesting sister-circuits. The efficiency curves $f_1(x)$ and $f_2(x)$ belong to LPD and HPD circuits, respectively. The crossover point, γ, is the point where one of these two circuits become the lead contributor to the total harvested energy. Thus, the LPD is operational if the RF input power is lower than γ, otherwise the HPD circuit is operational.

As shown in Fig. 7, there are $(\beta - \alpha)/stepsize$ potential crossover points between α and β. At each particular crossover point γ, the total area under efficiency curve is the cumulative

sum of the area under the two distinct efficiency curves corresponding to the LPD and HPD designs, one on either side of the crossover point γ. The total area under efficiency curve is hence

$$\text{Area}_{\text{total}} = \int_{\alpha}^{\gamma} f_1(x)\,\mathrm{d}x + \int_{\gamma}^{\beta} f_2(x)\,\mathrm{d}x. \tag{4}$$

The crossover point, γ, can be determined as follows:

$$\gamma = \arg\max_{\gamma}\left\{\int_{\alpha}^{\gamma} f_1(x)\,\mathrm{d}x + \int_{\gamma}^{\beta} f_2(x)\,\mathrm{d}x\right\}. \tag{5}$$

A problem is said to have an optimal substructure if an optimal solution can be constructed efficiently from optimal solutions to its subproblems. We claim that this optimization also exhibits the optimal substructure property. The proof is presented as follows:

Lemma:

$$\int_{\alpha}^{\gamma} f_1(x)\,\mathrm{d}x + \int_{\gamma}^{\beta} f_2(x)\,\mathrm{d}x \quad \text{is maximum then} \int_{\alpha}^{\gamma} f_1(x)\,\mathrm{d}x \quad \text{and} \int_{\gamma}^{\beta} f_2(x)\,\mathrm{d}x \quad \text{are maximum as well.} \tag{6}$$

Proof: if $\int_{\alpha}^{\gamma} f_1(x)\,\mathrm{d}x$ and $\int_{\gamma}^{\beta} f_2(x)\,\mathrm{d}x$ were not maximum, then we could substitute $\int_{\alpha}^{\gamma} f_1(x)\,\mathrm{d}x$ and $\int_{\gamma}^{\beta} f_2(x)\,\mathrm{d}x$ with larger values and hence obtain an even larger total area, $\int_{\alpha}^{\gamma} f_1(x)\,\mathrm{d}x + \int_{\gamma}^{\beta} f_2(x)\,\mathrm{d}x$.

Furthermore, the efficiency curve is also a function of impedance matching network, consisting of inductor (L) and capacitor (C). This implies that for each particular crossover point, there exists more than one efficiency curve. It can be represented in mathematical form as follows:

$$\forall\, \alpha : f(x) = f(L, C). \tag{7}$$

Consequently, the (5) becomes

$$\gamma = \arg\max_{\gamma}\left\{\int_{\alpha}^{\gamma} f_1(L, C, x)\,\mathrm{d}x + \int_{\gamma}^{\beta} f_2(L, C, x)\,\mathrm{d}x\right\}. \tag{8}$$

Finally, the number of rectifier stages influences the minimum required voltage at the input in order to obtain a certain output sufficient to drive a sensor mote. We consider various number of rectifier stages (N), ranging from 1 to 12 stages in this optimization framework. Hence, the (8) becomes

$$\gamma = \arg\max_{\gamma}\left\{\int_{\alpha}^{\gamma} f_1(N_1, L, C, x)\mathrm{d}x + \int_{\gamma}^{\beta} f_2(N_2, L, C, x)\mathrm{d}x\right\}. \tag{9}$$

We can construct the general optimization framework as follows:

$$\text{Given} : L, C, N \tag{10}$$

$$\text{To find} : \alpha, N_1, N_2 \tag{11}$$

$$\text{To Maximize} : \quad \text{Area}_{\text{total}} = \int_{\alpha}^{\gamma} f_1(N_1, L, C, x)\,\mathrm{d}x + \int_{\gamma}^{\beta} f_2(N_2, L, C, x)\,\mathrm{d}x$$

$$\text{Subject to} : \int_{\alpha}^{\gamma} f_1(N_1, L, C, x)\mathrm{d}x > \int_{\gamma}^{\beta} f_1(N_1, L, C, x)\mathrm{d}x \quad \text{and} \quad \int_{\gamma}^{\beta} f_2(N_2, L, C, x)\mathrm{d}x > \int_{\alpha}^{\gamma} f_2(N_2, L, C, x)\mathrm{d}x \tag{12}$$

$$\forall\, x : I(x + \Delta x) \geq I(x) \tag{13}$$

$$\forall\, x : V(x + \Delta x) \geq V(x) \tag{14}$$

$$V(x = -10) \geq 1.8\ \text{V}. \tag{15}$$

The aim of this optimization framework is to maximize area under the joint efficiency curve throughout, subject to several constraints which are explained below.

- The efficiency curves of both circuits, one optimized for low input power operation, i.e., the LPD, and another for high-power operation, i.e., HPD, should not overlap completely as the effective operational range of the circuit will be adversely impacted. This is possible by enforcing the constraint on having majority of the area under the efficiency curve to the left of the crossover point for the LPD circuit, while HPD circuit has majority of the area to the right of the crossover point.
- Voltage and current should be monotonically increasing. This places a constraint on the efficiency curve of the energy harvesting circuit to be continuous and without sudden breaks.
- Finally, the output voltage at $-20\ \text{dBm} \geq 1.8\ \text{V}$. This is to ensure that at the energy harvesting circuit is operable at the point where it is practically required to drive the sensor mote in the active state.

V. Simulation Results

The energy harvesting circuit is simulated using Agilent Advanced Design System (ADS) software. We use the *harmonic balanced analysis* (a frequency domain method) in this work since our objective is to compute the steady state solution of a nonlinear circuit. The alternate method, the so called *transient analysis* that is undertaken in the time domain is not used owing to the reason that it must collect sufficient samples for the highest frequency component. This involves significant memory and processing requirements.

For the optimization framework, we vary the crossover point throughout the target range, each time evaluating if the overall efficiency is optimized. The number of energy harvesting stages is varied from 1 to 12 for both LPD and HPD circuits. Moreover, components in the corresponding matching network are tuned to yield the maximum efficiency for a given choice of crossover point. We use the input power step size of 0.25 dBm in this paper for fine grained analysis.

In the first study, we keep the crossover point fixed and observe the resulting changes in the efficiency curves when the number of stages varies, as shown in Fig. 8. We vary the number of stages from 5 ,7, and 9 for the LPD, while HPD stages are 8, 10, and 12. The optimal choice of the circuit stages at a given crossover point is that which maximizes the overall efficiency η_o. The value of η_o, as well the conversion efficiency area for the two sister-circuits are shown in Table I. For the LPD, the value of the area under the efficiency curve increases as the number

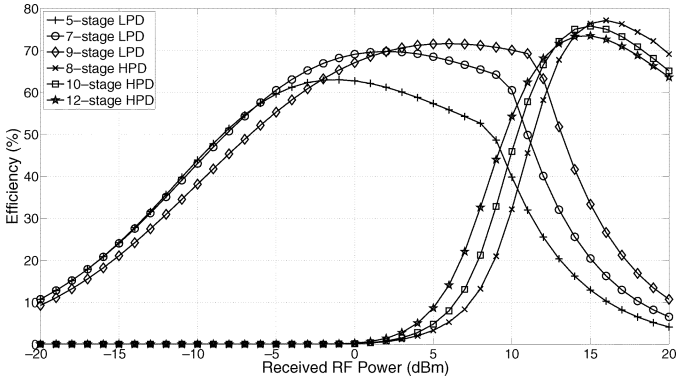

Fig. 8. Efficiency Comparison at 10.75 dBm for different sub-circuit stages.

TABLE I
NORMALIZED AREA AT 10.75 dBmCROSSOVER POINT

Sub-circuit	Number of stages/Area		
LPD	5-stage/1508.589	7-stage/1550.420	9-stage/1507.892
HPD	8-stage/722.535	10-stage/745.355	12-stage/745.222

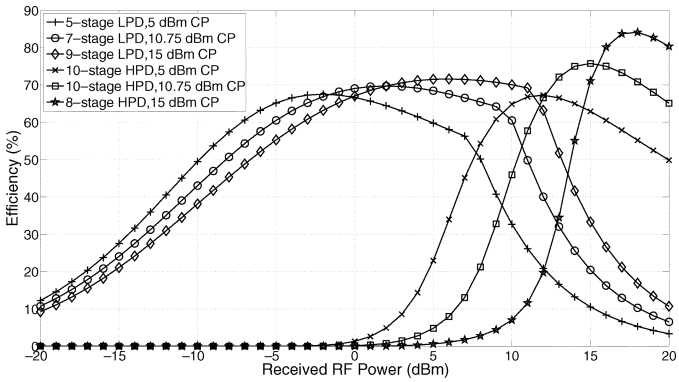

Fig. 9. Optimal efficiency comparison at different crossover.

TABLE II
OPTIMAL SOLUTION AT VARIOUS CROSSOVER POINTS

Sub-circuit/Area	5 dBm	10.75 dBm	15 dBm
LPD	5-stage/1268.209	7-stage/1550.420	9-stage/1767.046
HPD	10-stage/886.416	10-stage/745.355	8-stage/482.067
Total area	2154.625	2295.775	2249.122

of stages increases from 5 to 7. However, its peak efficiency reduces as additional stages are introduced. We observe that the optimal solution for the LPD is composed of seven-stages. Likewise, ten-stages are found to be best for the HPD. Consequently, the overall optimal solution, in the rage of -20 to 20 dBm, consists of the pair of seven-stage LPD circuit and ten-stage HPD circuit.

Next, the behavior of the proposed circuit for three different crossover points of 5, 10.75, and 15 dBm are plotted in Fig. 9. The optimal solution at 5 dBm crossover point consists of the pair of five-stage for the LPD circuit and ten-stages for the HPD circuit. Similarly, a nine-stage LPD circuit and eight-stage HPD circuit is the optimal solution set at 15 dBm crossover point. During the sweep of the crossover point from the lower input power end -20 dBm to upper end 20 dBm, we select the optimal solution as one that yields the maximum η_o. Table II shows the normalized η_o for various crossover points.

Through an exhaustive search following the constraints of our optimization framework, we find that the seven-stage low-LPD

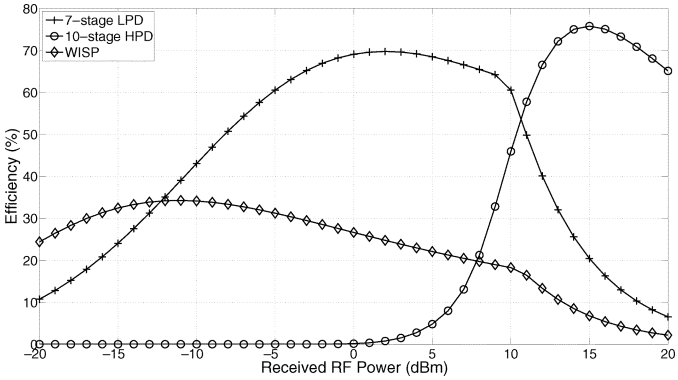

Fig. 10. Efficiency of optimized energy harvesting circuit and WISP.

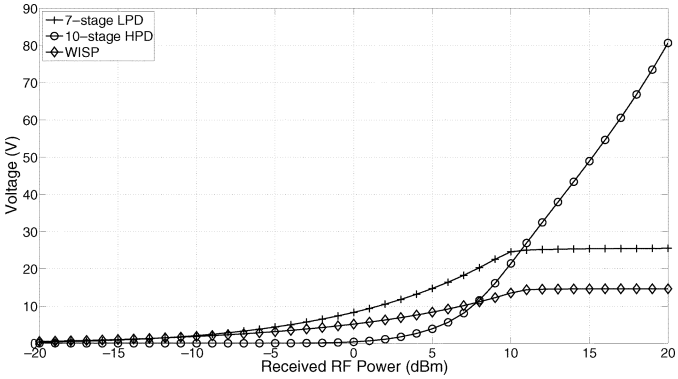

Fig. 11. Output voltage of optimized energy harvesting circuit and WISP.

circuit and the ten-stage HPD circuit, with the crossover point of 10.75 dBm, yields the maximum η_o, and hence, this is the optimal solution to the framework. The efficiency curves and the subsequent normalized area values are included in Fig. 10 and Table II, respectively.

In order to show the benefit of the proposed dual-stage design, we compare our design with Intel research's Wireless Identification and Sensing Platform (WISP) [17]. WISP power harvester consists of a four-stage charge pump and it employs Agilent HSMS-285C schottky diodes which is similar to that of our design. We use schematic and components' parameters as published in [17]. Consequently, it is fair to say that the performance difference is the result of the design and optimization. Note that WISP uses the zener diode, connected in shunt configuration with the load, to regulate the output voltage. For this performance evaluation purpose, it is omitted from the simulation. Fig. 10 shows the efficiency plots of WISP and dual-stage design. It is clear that the dual-stage design yields much higher efficiency at -12 dBm onwards. The benefit of dual-stage design stands out in HPD region where the efficiency of WISP drastically drops. However, WISP outperforms the dual-stage design between -20 to -13 dBm. This is not surprising since we optimized the design to deliver optimal efficiency throughout the range of -20 to 20 dBm.

The output voltage of the optimized energy harvesting circuit and WISP are shown in Fig. 11. The energy harvesting circuit yields the output voltage of 2.074 V at -10 dBm. [13] has stated earlier that the Mica2 sensor mote is able to operate at 1.8 V. This output voltage of energy harvesting circuit at -10 dBm

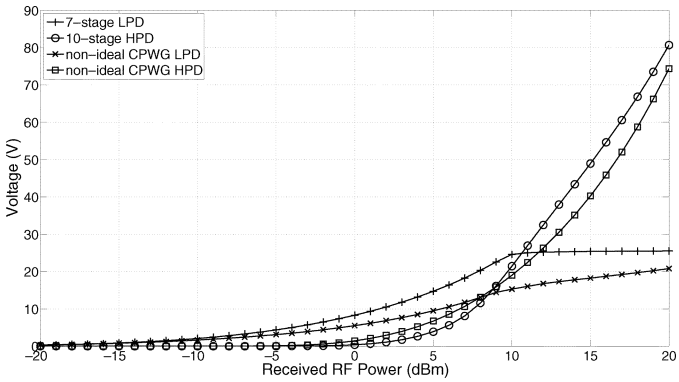

Fig. 12. Voltage comparison of ideal and nonideal circuit with PCB effect.

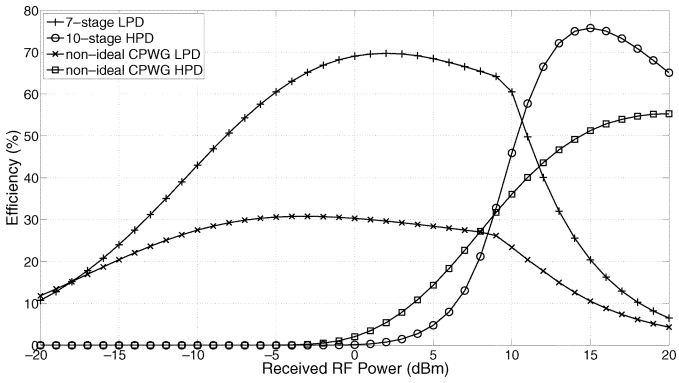

Fig. 13. Efficiency comparison of ideal and nonideal circuit with PCB effect.

is sufficient to fully operate the Mica2 sensor mote, once the energy storage is sufficiently charged. Moreover, at -7 dBm, the output current of the energy harvesting circuit is 32.91 μA. It implies that the energy harvesting circuit is able to directly supply the power to deep-sleep Mica2 sensor mote, on the basis that the energy storage is sufficiently charged, which requires no more than 30 μA. The energy neutral operation can be sustained in the latter case.

VI. Fabrication and Evaluation

The simulation results obtained previously are under an assumption that all components, except Schottky diodes, exhibit an ideal behavior. With nonideal components and parasitic effects, this is rarely achievable in practice. Consequently, it is imperative that all related parasitic parameters and precise models of components have to be incorporated into the simulation. This not only yields a closer result to that of the prototype but also provides an upper bound on achievable efficiency with respect to a particular prototype design. For this purpose, Agilent ADS simulation with co-planar waveguide with ground plane (CPWG) is used to observe the effect of the PCB. Moreover, components are modeled with ADS and vendor supplied component libraries. The voltage and efficiency comparison between ideal circuit and nonideal circuit with PCB effect are shown in Figs. 12 and 13, respectively. The effect of nonideal components and PCB becomes clear as the received RF input power goes beyond -16 dBm. This implies that the fabrication method plays an important role on the performance of the energy harvesting circuit. It is preferable to choose the

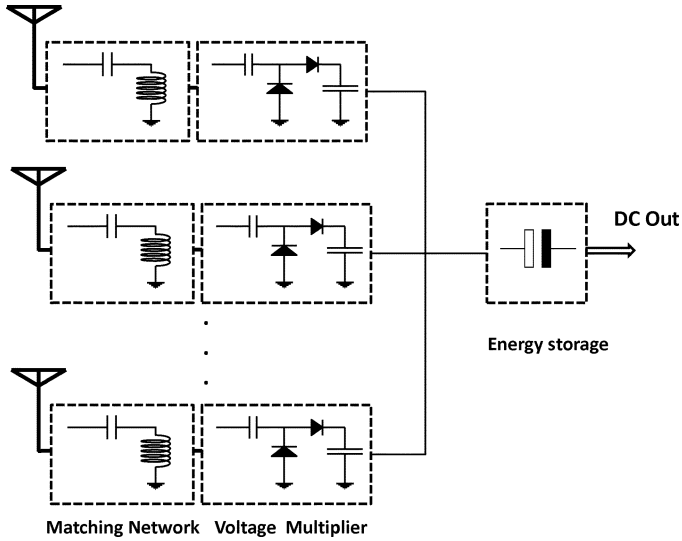

Fig. 14. RF energy harvesting with multiple antennas.

fabrication method that yields the least parasitic effects as well as minimizes the effect of the components' layout. "System on Chip" (SoC) is a highly recommended fabrication method, which however lies beyond the scope of this paper.

With the effect of nonideal components and PCB, it is unlikely that one can achieve the optimal result obtained in the optimization section. We propose the use of multiple antennas in addition to the existing circuit. Consequently, the amount of energy harvested can be increased depending on number of antennas implemented. Fig. 14 shows the energy harvesting with multiple input antennas concept. Each antenna collects its own signal, connects to its own matching network and voltage multiplier. However, they all share the energy storage. Note that this concept does not increase conversion efficiency of the circuit since the efficiency of the circuit remains the same. However, the amount of harvested energy to area ratio is increased. The voltage and efficiency of circuits with multiple antennas are shown in Figs. 15 and 16, respectively. It is obvious that both voltage and efficiency of the circuit can be increased by introducing additional antennas. However, the gain increase is not linear and reduces drastically with additional antennas introduced. This limits the amount of multiple antennas used for the purpose of energy harvesting enhancement.

The final fabricated PCB of our proposed energy harvesting module connected to a Mica2 mote is shown in Fig. 17. The PCB is fabricated with FR-4 epoxy glass substrate and has two layers, one of which serves as a ground plane. The prototype consists of the design obtained from the proposed optimization. We select components with values and ratings of their performance parameter as close as possible to ones obtained from the simulation. This data is summarized in Table III.

The energy harvesting circuit prototype is tuned to match simulation parameters using Agilent E5061B vector network analyzer. In order to measure dc power output from the prototype, Agilent N5181 MXG RF signal generator is used to provide a known RF power to the prototype from -20 to 20 dBm. The dc output power from the prototype is obtained from measuring the voltage and current associated with the resistive load of 100 KΩ.

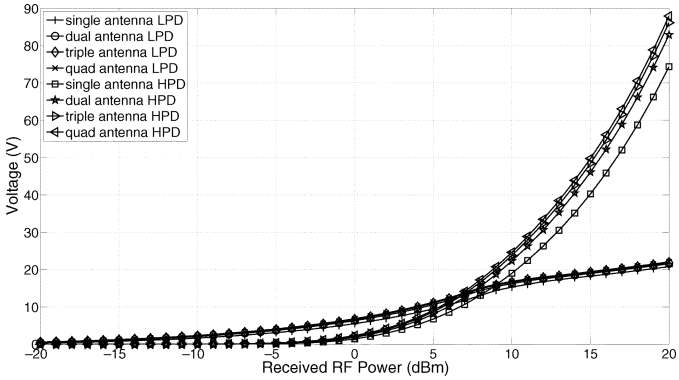

Fig. 15. Effect of multiple antennas on EH circuit's voltage.

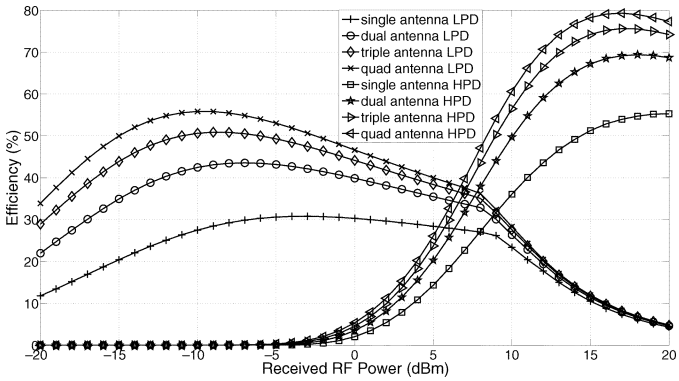

Fig. 16. Effect of multiple antennas on EH circuit's efficiency.

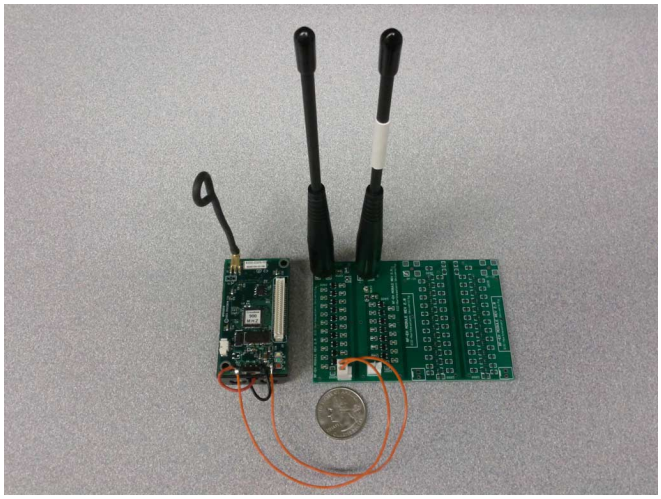

Fig. 17. RF energy harvesting circuit prototype.

TABLE III
COMPONENTS USED IN ADS SIMULATION

Component	Value
Inductor	3.0, 7.12 nH
Capacitor	1.5, 2.9 pF
Stage capacitor	36 pF
Diode	HSMS-2852, HSMS-2822

The load value representing the Mica2 is so chosen as it is measured in sleep mode to consume 30 μA at 3.0 V, which translates to a 100 KΩ resistive load. We use Agilent 34401A multimeter to measure voltage and current on the resistive load. Our prototype is fabricated with specifications shown in Table IV.

TABLE IV
PARAMETERS USED IN PCB FABRICATION

Component	Value
Laminate thickness	62 mil FR-4
Number of Layers	2-layer, one serves as a ground plane
Copper thickness	1.7 mil
Trace width	20 mil with 12 mil gap
Dielectric constant	4.6
Through-hole size	29 mil

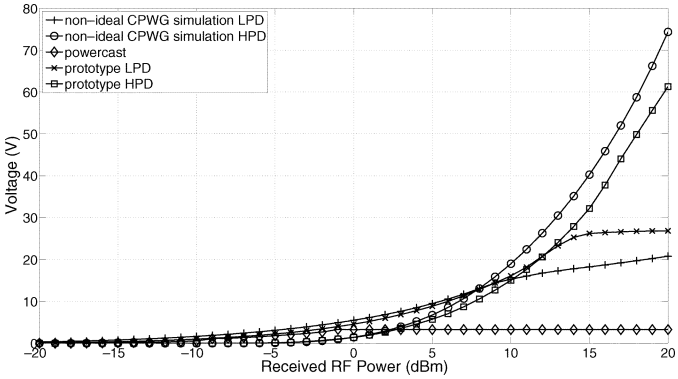

Fig. 18. Output voltage comparison of simulation, prototype and powercast energy harvesting circuit.

We describe the efficiency of our fabricated harvesting board, also referred to as *prototype*, and compare with the commercially available RF energy harvester from Powercast [16]. We use P1100 evaluation board for the performance comparison. Powercast P1100 is a high efficiency RF energy harvesting device that converts received RF energy into dc power. The voltage and current of Powercast P1100 is measured with the same equipments under the same external conditions.

Fig. 18 shows the voltage plot of the nonideal simulation, prototype and Powercast P1100 across the load of 100 KΩ with -20 to 20 dBm input RF power. It is clear that the voltage plots of the prototype, both LPD and HPD, are not able to exceed with the simulation results, though they both closely follow the voltage plots of the simulation with nonideal components with PCB effect and exhibit similar behavior.

Fig. 19 depicts comparison of output voltage plots of our prototype in LPD region against the Powercast P1100 energy harvesting circuit. The proposed prototype provides a higher voltage than the Powercast P1100 throughout the range of -20 to 20 dBm. At -1 dBm, the output voltage of Powercast P1100 holds constant at 3.3 V. This is because the Powercast P1100 has the voltage regulator built into the package and it starts to regulate its output voltage at -1 dBm with the voltage of 3.3 V.

Fig. 20 shows the efficiency comparison of non-ideal simulation, prototype and Powercast P1100 across the load of 100 KΩ with -20 dBm to 20 dBm input RF power. In order to measure the efficiency of the Powercast P1100 beyond -1 dBm, the output voltage of the Powercast P1100 is controlled under 3.3 V by varying amount of current drawn by the load. The efficiency plots precisely correspond to the voltage plots described previously. The efficiency plots of the prototype exhibit similar behavior when compared to nonideal simulation values, except

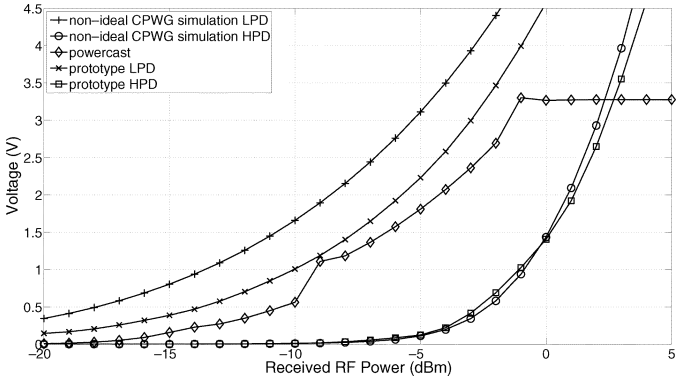

Fig. 19. Output voltage comparison of simulation, prototype and powercast energy harvesting circuit.

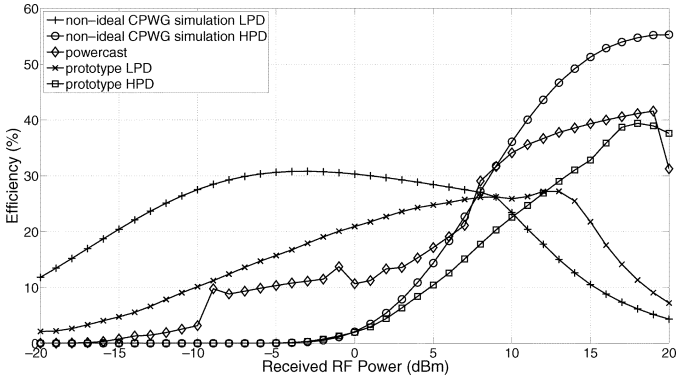

Fig. 20. Efficiency comparison of simulation, prototype and powercast energy harvesting circuit.

in the limited range of input power in which the LPD shows a comparatively high deviation between simulation and experimental results. This occurs owing to the inability of capturing parasitic capacitances, resulting from PCB manufacturing and components' tolerance.

It is interesting to investigate feasible applications under extremely low power range, -20 to 0 dBm. The prototype gives the output voltage of 1 V at -10 dBm and 1.9234 V at -6 dBm, respectively. At these two particular points, the prototype has the efficiency of 10% and 14.73% which are 10 μW and 37 μW, respectively. With the advancement in extremely low power micro-controller (MCU), the power consumption continues to decrease. For example, Texas Instruments' MSP430L092 can operate at the voltage as low as 0.9 V and consumes 3 μA in LPM4 mode, which translates to 2.7 μW [18]. Consequently, the prototype can directly supply power to sustain the operation of MSP430L092 at as low as -10 dBm received RF power. Similarly, Mica2 sensor node is able to operate in power-down mode at -6 dBm received RF power.

The application is not only limited to powering sensors directly but also trigger charging, energy neutral operation and radio wakeup [19]. In trigger charging operation, the surplus energy beyond sensor's consumption is accumulated in energy storage, i.e., super capacitor and rechargeable battery, thus increases the sensor's lifetime. For example, Texas Instruments' MSP430G2553 [20] in LPM4 mode draws 100 nA at 1.8 V, which translates to 180 nW. The prototype yields 2.5% efficiency at -20 dBm, which is 250 nW. In energy neutral operation which the rate of energy consumption is less than or equal to that of the harvesting, the prototype is able to sustain the energy neutral of MSP430G2553 in LPM4 at -20 dBm. Finally, the energy harvesting circuit can be used to wake up the sensor node when predetermined signal strength is detected in the proximity. In this case, the sensor node has its own power source and spends most of the time in power-down mode. As a result, the sensor's lifetime is extended with the use of energy harvesting radio wakeup.

With most applications the output power needs to be regulated. However, voltage regulation may not be of concern under some circumstances. For example, the high voltage produced by the circuit occurs under the assumption that the sensor is in power-down mode. Once the sensor wakes up, it draws higher current thus the voltage decreases. With ambient RF energy harvesting, the input voltage range is limited by the ambient RF, which rarely exceeds 0 dBm. So it is safe to say the output voltage is bounded and voltage regulator is not necessary. However, using a voltage regulator to regulate the output to a useful voltage is recommended for most applications. A simple zener diode, in shunt configuration with the load, can be used to regulate the output voltage similar to WISP design. Otherwise, a buck converter with large conversion ratio can be used for this purpose.

VII. Conclusion

We show that with a simple yet optimal design and optimization, the prototype can yield almost double the efficiency than that of a major commercially available energy harvesting circuit in the low incident power range (simulation results for the circuit reveal about 70% operational efficiency). Our study implies that Mica2 sensor motes can be perpetually operated when their duty-cycle is carefully selected based on the incident RF power (as low as -6 dBm). Moreover, the prototype is able to sustain the energy neutral of Texas Instruments' MSP430G2553 in LPM4 at -20 dBm. The experimental results are in good agreement with the values seen in the nonideal simulation. We also compare our prototype's efficiency with the commercially available RF energy harvester from Powercast, where our prototype largely outperforms the Powercast P1100 in the range of -20 to 7 dBm. Finally, in order to have a performance improved and lower cost, the circuit needs to be implemented as "System on Chip" as it suffers less above mentioned parasitics, and we will pursue this in our future work.

References

[1] N. Tesla, "The transmission of electric energy without wires," in *13th Anniversary Number of the Electrical World and Engineer*, 1904.
[2] J. Curty, M. Declercq, C. Dehollain, and N. Joehl, *Design and Optimization of Passive UHF RFID Systems*. New York: Springer, 2007.
[3] J. A. Paradiso, "Systems for human-powered mobile computing," in *Proc. 43rd Design Automation Conf. (DAC)*, Jul. 24–28, 2006, pp. 645–650.
[4] C. R. V. Leonov, T. Torfs, P. Fiorini, and C. Van Hoof, "Thermoelectric converters of human warmth for self-powered wireless sensor nodes," *IEEE Sensors J.*, vol. 7, no. 5, pp. 650–657, May 2007.
[5] K. Lin, J. Yu, J. Hsu, S. Zahedi, D. Lee, J. Friedman, A. Kansal, V. Raghunathan, and M. Srivastava, "Heliomote: Enabling long-lived sensor networks through solar energy harvesting," in *3rd Int. Conf. Embedded Networked Sensor Syst.*, Nov. 2–4, 2005, p. 309.

[6] A. Sample and J. R. Smith, "Experimental results with two wireless power transfer systems," in *IEEE Radio Wireless Symp.*, Jan. 2009, pp. 16–18.
[7] D. W. Harrist, "Wireless battery charging system using radio frequency energy harvesting," M.S. thesis, Univ. Pittsburgh, Pittsburgh, PA, 2004.
[8] M. M. Tentzeris and Y. Kawahara, "Novel energy harvesting technologies for ICT applications," in *IEEE Int. Symp. Appl. Internet*, 2008, pp. 373–376.
[9] T. Ungan and L. M. Reindl, "Harvesting low ambient RF-sources for autonomous measurement systems," in *Proc. IEEE Int. Instrum. Meas. Technol. Conf.*, May 2008, pp. 62–65.
[10] H. Javaheri and G. Noubir, "iPoint: A platform-independent passive information kiosk for cell phones," in *Proc. 7th IEEE SECON 2010*, Jun. 2010, pp. 1–9.
[11] FCC Codes of Regulation, Part 15 [Online]. Available: http://www.access.gpo.gov/nara/cfr/waisidx03/
[12] H. Yan, J. G. M. Montero, A. Akhnoukh, L. C. N. de Vreede, and J. N. Burghart, "An integration scheme for RF power harvesting," presented at the 8th Annu. Workshop Semiconductor Advances Future Electron. Sensors, Veldhoven, The Netherlands, 2005.
[13] R. Doost, K. Chowdhury, and M. Di Felice, "Routing and link layer protocol design for sensor networks with wireless energy transfer," in *IEEE Globecom*, Dec. 2010, pp. 1–5.
[14] J. Curty, N. Joehl, C. Dehollain, and M. Declercq, "Remotely powered addressable UHF RFID integrated system," *IEEE J. Solid-State Circuits*, vol. 40, no. 11, pp. 2193–2202, Nov. 2005.
[15] D. Bouchouicha, F. Dupont, M. Latrach, and L. Ventura, "Ambient RF energy harvesting," in *IEEE Int. Conf. Renewable Energies Power Quality (ICREPQ'10)*, Mar. 2010, pp. 486–495.
[16] P2000 Series 902–928 MHz Powerharvester Development Kit Powercast Corp. [Online]. Available: http://www.powercastco.com/products/development-kits/
[17] *Wireless Identification and Sensing Platform (WISP)*, [Online]. Available: http://wisp.wikispaces.com/
[18] *Texas Instruments MSP430L092*, [Online]. Available: http://www.ti.com/product/msp430l092
[19] H. Ba, I. Demirkol, and W. Heinzelman, "Feasibility and benefits of passive RFID wake-up radios for wireless sensor networks," in *IEEE GolbeCom 2010*, Dec. 2010, pp. 1–5.
[20] *Texas Instruments*, MSP430G2553 [Online]. Available: http://www.ti.com/product/MSP430G2553

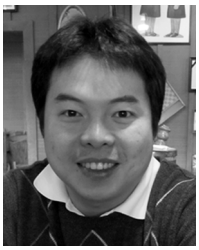

Prusayon Nintanavongsa (S'12) received the B.E.E. degree from SIIT, Bangkok, Thailand, in 1999, the M.E.E. degree from KMUTT, Bangkok, Thailand, in 2001, the M.S.E.E. degree from Boston University, Boston, MA, in 2006. He is currently working toward the Ph.D. degree in computer engineering at Northeastern University, Boston, MA.

He is a Research Assistant in the Electrical and Computer Engineering Department at Northeastern University, Boston, MA. His research interests include RF energy harvesting circuit design, protocol design in energy harvesting wireless sensor networks, and ultra-low power wireless sensor networks.

Mr. Nintanavongsa is a recipient of the Royal Thai government scholarship.

Ufuk Muncuk received the B.S. degree in electrical and electronics engineering from Firat University, Elazig, Turkey, in 2008, and the M.S. degree in electrical and electronics engineering from Erciyes University, Kayseri, Turkey, in 2009. He started the M.S. degree in electrical and computer engineering at Northeastern University, Boston, MA, on National Education Ministry of Turkey scholarship, in 2010.

His research interests include circuit design for RF energy harvesting systems, wireless sensor networks, and cognitive radio systems.

David Richard Lewis received the B.S. degree in electrical engineering and minor in business administration, in 2008, from Northeastern University, Boston, MA, where he is currently working toward the M.S. degree in electrical engineering with a concentration in electronic circuits, semiconductor devices, and microfabrication.

He started his professional career at Oasis Semiconductor in 2005. He has worked for Sigmatel, Freescale, and currently for Conexant Systems as a hardware and Systems Design Engineer

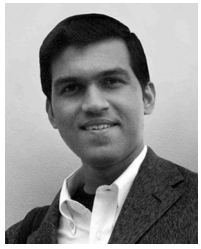

Kaushik Roy Chowdhury (M'09) received the B.E. degree in electronics engineering with distinction from VJTI, Mumbai University, India, in 2003, and the M.S. degree in computer science from the University of Cincinnati, Cincinnati, OH, in 2006, and the Ph.D. degree from the Georgia Institute of Technology, Atlanta, in 2009. His M.S. thesis was given the outstanding thesis award jointly by the Electrical and Computer Engineering and Computer Science Departments at the University of Cincinnati.

He is Assistant Professor in the Electrical and Computer Engineering Department at Northeastern University, Boston, MA. He currently serves on the editorial board of the Elsevier *Ad Hoc Networks* and Elsevier *Computer Communications* journals. His expertise and research interests lie in wireless cognitive radio *ad hoc* networks, energy harvesting, and multimedia communication over sensors networks.

Dr. Chowdhury won the best paper award in the Ad Hoc and Sensor Networks symposium at the IEEE ICC conference in 2009.